

## Supporting Information for Ultrafast and stable phase transition realized in MoTe<sub>2</sub>-based memristive devices

Hui-Kai He,<sup>a,b</sup> Yong-Bo Jiang,<sup>b</sup> Jun Yu,<sup>b</sup> Zi-Yan Yang,<sup>a</sup> Chao-Fan Li,<sup>c</sup> Ting-Ze Wang,<sup>a,b</sup> De-Quan Dong,<sup>a,b</sup> Fu-Wei Zhuge,<sup>b</sup> Ming Xu,<sup>a</sup> Zhi-Yi Hu,<sup>c</sup> Rui Yang,<sup>\*a,b</sup> Xiang-Shui Miao<sup>\*a</sup>

<sup>a</sup>Wuhan National Laboratory for Optoelectronics, School of Optical and Electronic Information, School of Integrated Circuits, Huazhong University of Science and Technology, Wuhan, China.

<sup>b</sup>State Key Laboratory of Material Processing and Die & Mould Technology, School of Materials Science and Engineering, Huazhong University of Science and Technology, Wuhan, China.

<sup>c</sup>State Key Laboratory of Advanced Technology of Materials Synthesis and Processing, NRC (Nanostructure Research Centre), Wuhan University of Technology, China.

Email: [yangrui@hust.edu.cn](mailto:yangrui@hust.edu.cn), [miaoxs@hust.edu.cn](mailto:miaoxs@hust.edu.cn)

### 1. Fabrication process of the MoTe<sub>2</sub> memristive device

The fabrication process of the Au/Ti/MoTe<sub>2</sub>/Au/Ti memristive device is given in Fig. S1.

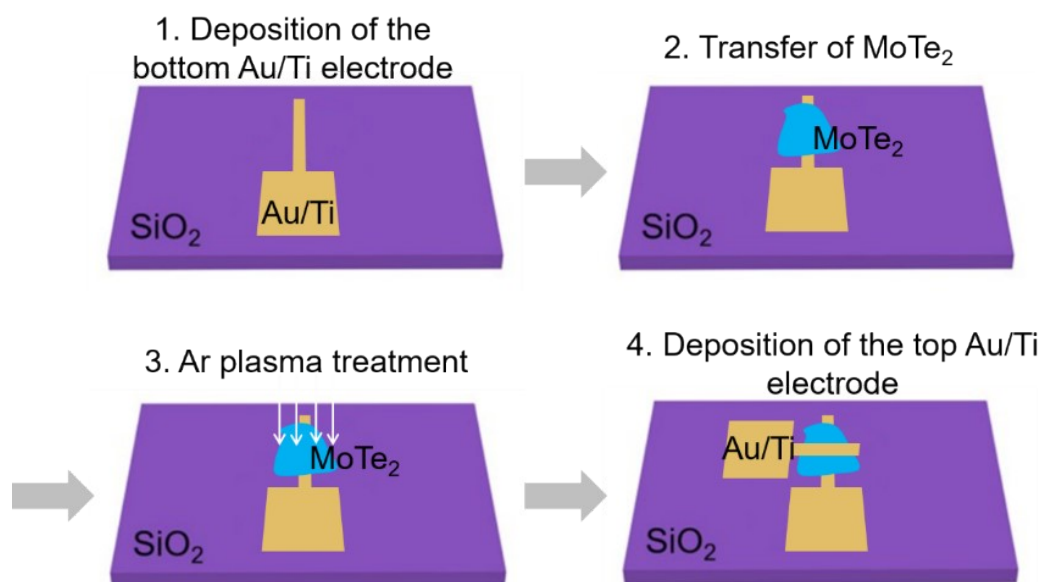


**Fig. S1** Fabrication process of the MoTe<sub>2</sub> memristive device.

### 2. Electroforming process

At the beginning, the current of the MoTe<sub>2</sub> device was low due to its high resistance. After the application of a relatively large negative voltage (about -4.0 V), the device switched to the

---

LRS. This process is named as electroforming. After the electroforming process, stable bipolar resistive switching was obtained when the voltage sweeping between -2.0 V and 1.5 V, as shown in Fig. S2.

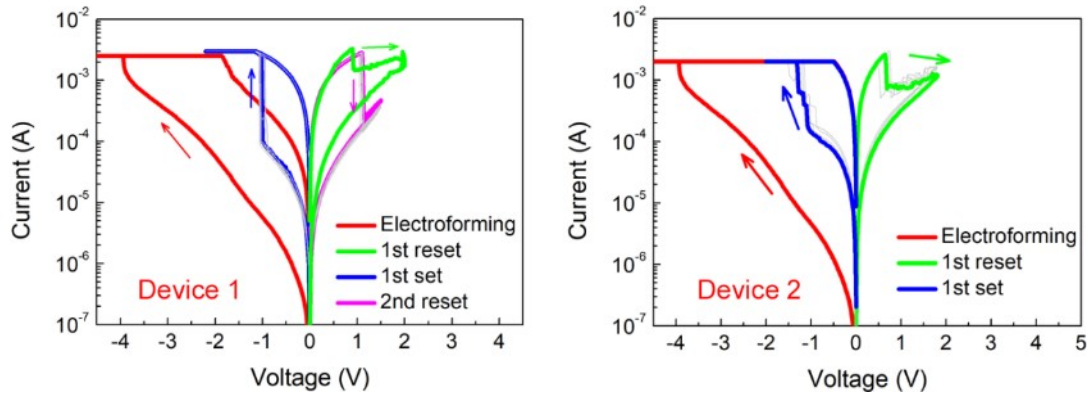


**Fig. S2** Typical  $I$ - $V$  curves of two  $\text{MoTe}_2$  memristive devices with electroforming processes.

### 3. Multi-level resistance states obtained through controlling the compliance currents

As shown in Fig. S3a, the resistance level of LRS can be controlled by adjusting the compliance currents. The higher SET compliance current, the lower resistance value of the device was achieved. Eight resistance states with good retention are obtained, see Fig. S3b.

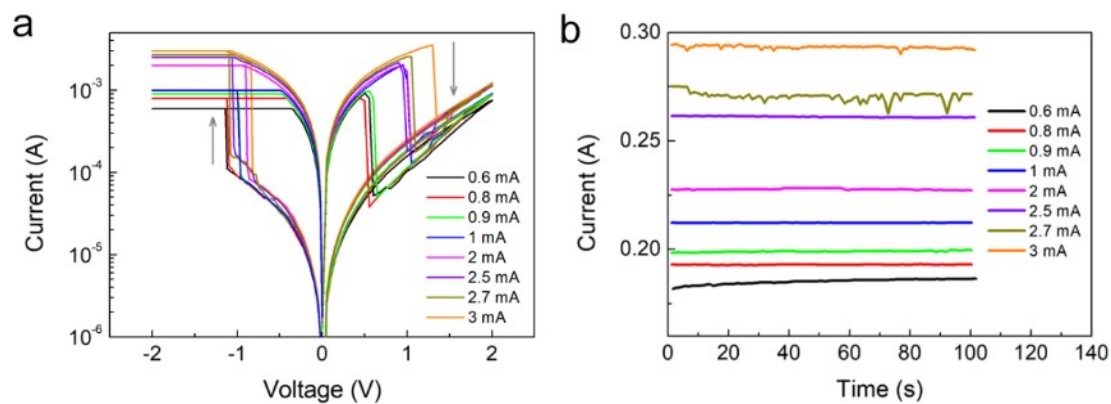


**Fig. S3 Multi-level resistance states.** (a)  $I$ - $V$  curves with different negative compliance currents ranging from 0.6 to 3 mA. (b) Eight resistance values obtained through changing the compliance currents.

#### 4. Electrical performance of the MoTe<sub>2</sub> devices with different flake thicknesses

The thickness of the MoTe<sub>2</sub> apparently affects the switching behavior, as shown in Fig. S4. For thin MoTe<sub>2</sub> (4.6 and 5 nm), the devices exhibited stable bipolar resistive switching behavior with narrow SET and RESET voltage distributions. However, the distributions of SET and RESET voltage become wide with the increasing of the MoTe<sub>2</sub> thickness. And, for thick MoTe<sub>2</sub> (80 nm), the resistive switching become unstable. For the MoTe<sub>2</sub> device with thick film, larger electric field is needed to induce the occurrence of phase transition. Upon the application of larger electric field, more Te vacancies migrate and accumulate in the local region, resulting in 1T' phase being quite stable, and difficult to recover back to 2H phase. Therefore, the device is easy to get stuck in LRS and cannot be switched back to HRS, so that the endurance remarkably degrades with thick MoTe<sub>2</sub> film.

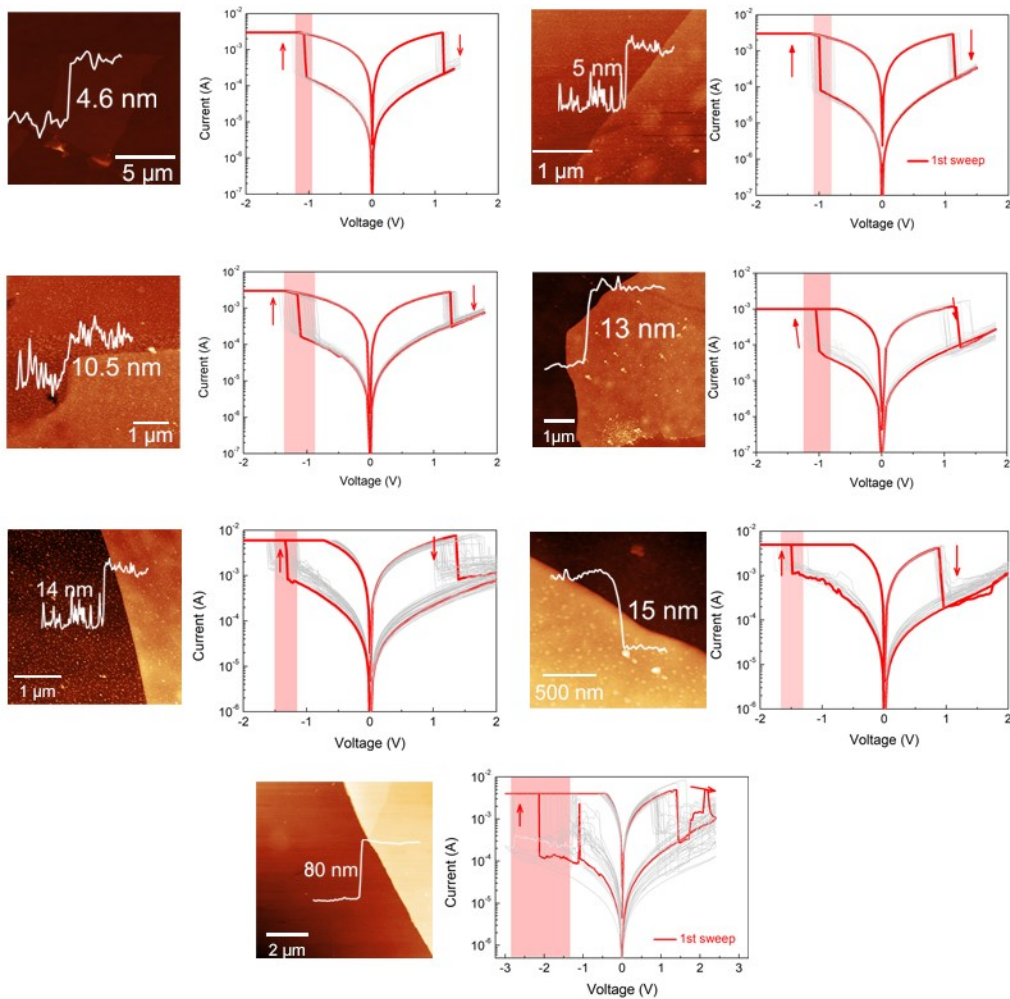


**Fig. S4** Electrical performance of the MoTe<sub>2</sub> devices with different flake thicknesses ranging from 4.6 to 80 nm.

## 5. Ultrafast SET and RESET cycles

As shown in Fig. S5, the device could be switched between the HRS and LRS over 50 cycles under the applied pulses with the width of 40 ns. There is a mixture of 2H and 1T' phases in the switching region in the LRS and HRS and the relative proportions of these two phases remains unchanged in the switching cycles. In the LRS, 1T' phase dominates the carrier transportation, resulting in stable LRS. In contrast, 2H phase dominates the carrier transportation in the HRS, a slight fluctuation in the residual amount of 1T' phase is unavoidable and might lead to an evident noise in the HRS, considering the 1T' phase has much significant effect on the resistance state. Notably, under the SET pulse with the width of 40 ns, Te vacancies migrate and accumulate in the local region, leading to the 2H-to-1T' phase transition. However, the number of Te vacancies accumulated in the phase transition region might be not enough, and the 1T'-MoTe<sub>2</sub> can easily recover back to 2H-MoTe<sub>2</sub>. Therefore, the device can only be switched for 50 cycles and easily stuck at HRS.

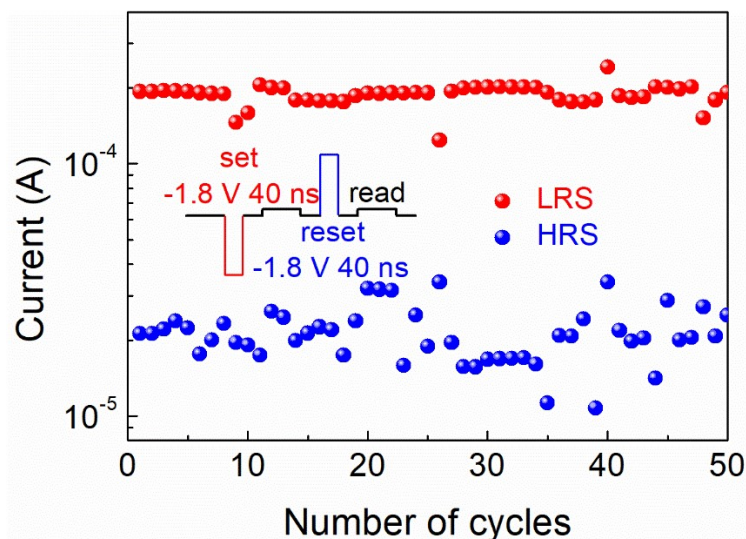


**Fig. S5** Ultrafast SET (-1.8 V/40 ns) and RESET (1.8 V/40 ns) operations up to 50 cycles.

## 6. The effect of electrodes on the switching behavior

In the maintext, Au/Ti layers were used as the top and bottom electrodes to prepare the MoTe<sub>2</sub> device. In order to understand the role of electrodes in the observed switching behavior, Au (without Ti adhesive layer) and graphene were used to replace the electrodes of Au/Ti layers. As shown in Fig. S6, similar switching behavior was observed in the Au/MoTe<sub>2</sub>/Au/Ti devices, indicating Ti layer is not involved in the switching process. Fig. S7 reports the switching behaviors observed in graphene/MoTe<sub>2</sub>/graphene devices. And similar and reproducible switching behaviors were obtained in these devices. As we all know, graphene is an excellent diffusion barrier for metals, ruling out the possibility of diffusion of metal atoms into the TMD layer that accounts for the resistive switching.

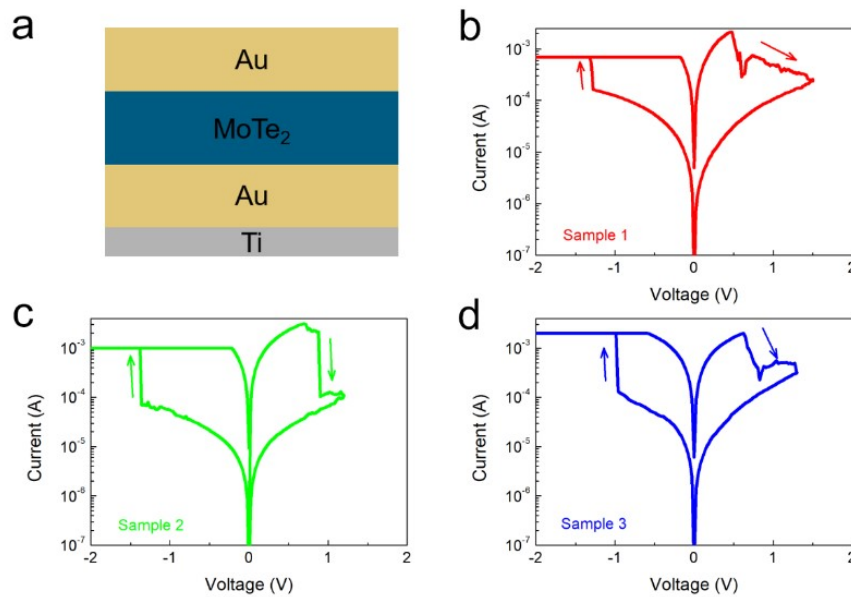


**Fig. S6** Schematic of device structure (a) and electrical performance of Au/MoTe<sub>2</sub>/Au/Ti devices (b, c, d, three samples).

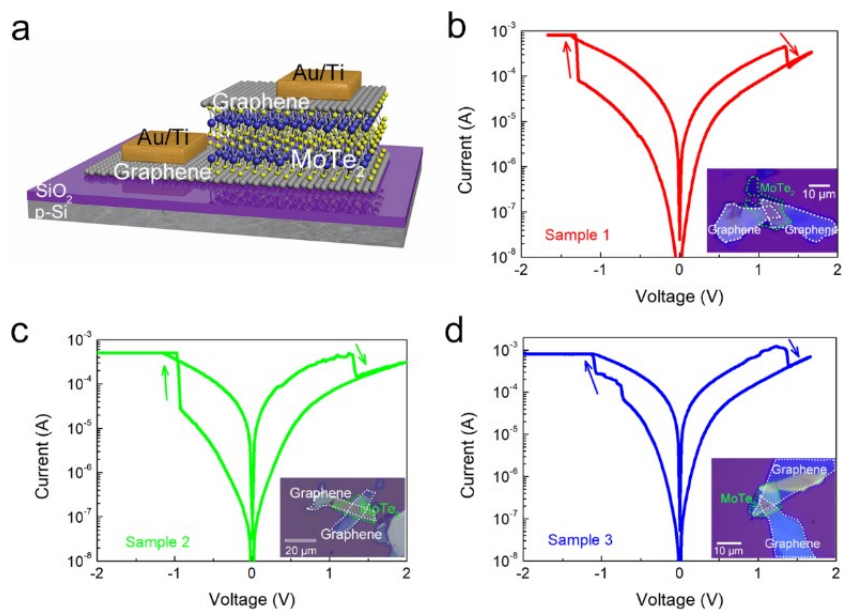


**Fig. S7** Schematic of device structure (a) and electrical performance of graphene/MoTe<sub>2</sub>/graphene devices (b, c, d, three samples).

## 7. Cross-sectional HRTEM to reveal structural changes of the MoTe<sub>2</sub> layer during the switching process

From Fig. S8, one can clearly observe some structural changes of the MoTe<sub>2</sub> layer occurred after the electroforming process. And, the interface of top Ti/MoTe<sub>2</sub> becomes blurred after electroforming. However, it is difficult for a general TEM (not a double spherical aberration TEM) to identify the change of crystal structure for layered materials from cross section.

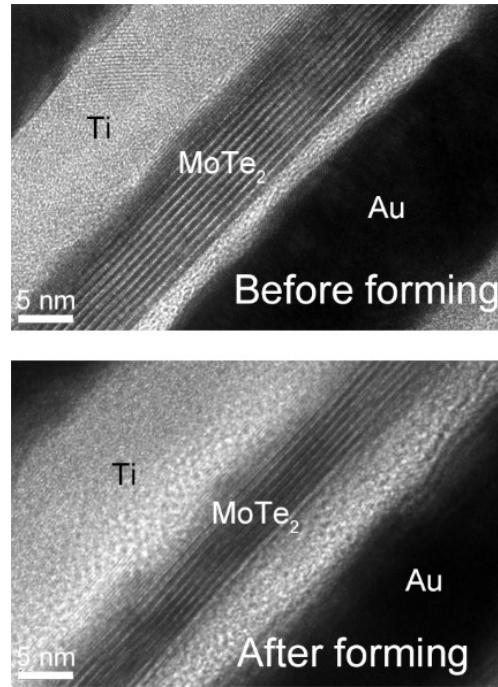


**Fig. S8** HRTEM of cross-sectional samples before and after electroforming.

#### 8. In-situ Raman analysis to reveal the switching mechanism

To locate the switching region, the whole area of the device was measured, as shown in Fig. S9. After electroforming, the device switched to LRS and a bright region appeared. Then the brightness of this region was markedly dimmed when the device switched back to HRS (see Fig. S9b). Note that these three Raman maps were collected based on the sum of Raman intensity counts in the range of  $100.4\text{-}150.1\text{ cm}^{-1}$ , corresponding to the  $A_g$  mode of  $1T'$ -MoTe<sub>2</sub>. Fig. S9c shows Raman spectra of the position marked with green cross in (b) at the pristine state, LRS and HRS. After electroforming, the peaks at  $124$  and  $138\text{ cm}^{-1}$  ( $A_g$  mode of  $1T'$ -MoTe<sub>2</sub>) appeared and the peak at  $233\text{ cm}^{-1}$  ( $E_{2g}$  mode of  $2H$ -MoTe<sub>2</sub>) decreased. Then, the peaks at  $124$  and  $138\text{ cm}^{-1}$  decreased drastically while the peak at  $233\text{ cm}^{-1}$  increased slightly when the device switched from LRS to HRS. These results directly demonstrate that the resistive switching is attributed to the phase transition between  $2H$  and  $1T'$  phases in MoTe<sub>2</sub>.

---

Fig. S10 reports the in-situ Raman analysis of another sample, showing similar results with those reported in above Fig. S9. Notably, it was found that phase transition occurred at the edge or corner of the switching layer in these devices. This preferential occurrence is reasonable, because a strong electric field forms at the corner or edge of the switching layer with sharp topological features.

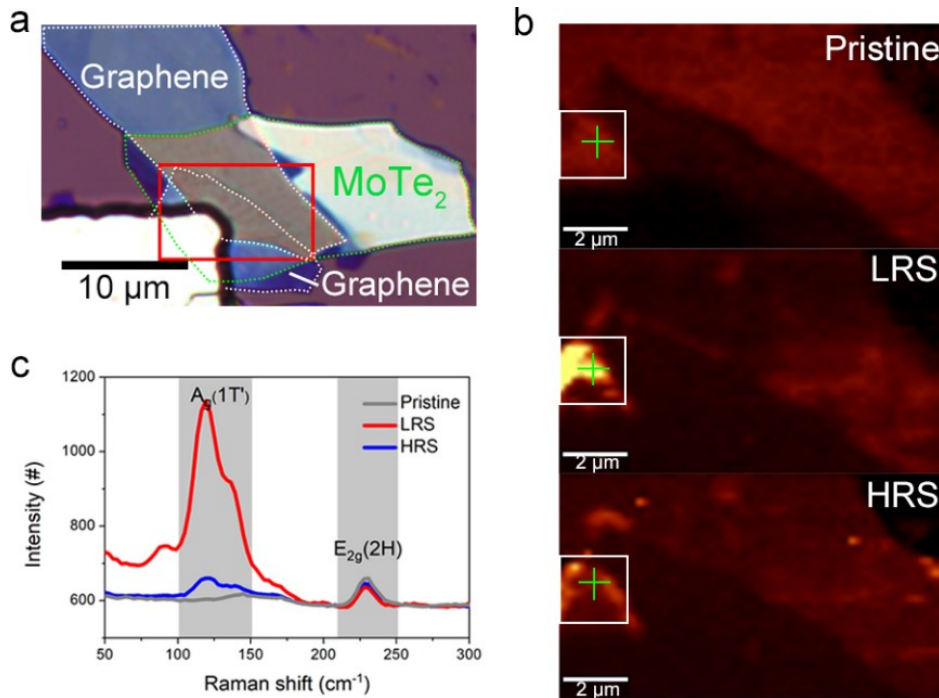


**Fig. S9 In-situ Raman analysis (the whole device).** (a) The optical image of the graphene/MoTe<sub>2</sub>/graphene device. The mapping area is marked with a red rectangle. (b) Three Raman maps correspond to the sum of Raman intensity counts in the range of 100.4-150.1 cm<sup>-1</sup> (indicating 1T' phase) at the pristine state, LRS and HRS, with a white rectangle indicating the region where the phase transition occurs. (c) Raman spectra of the position marked with green cross in (b) at the pristine state, LRS and HRS.

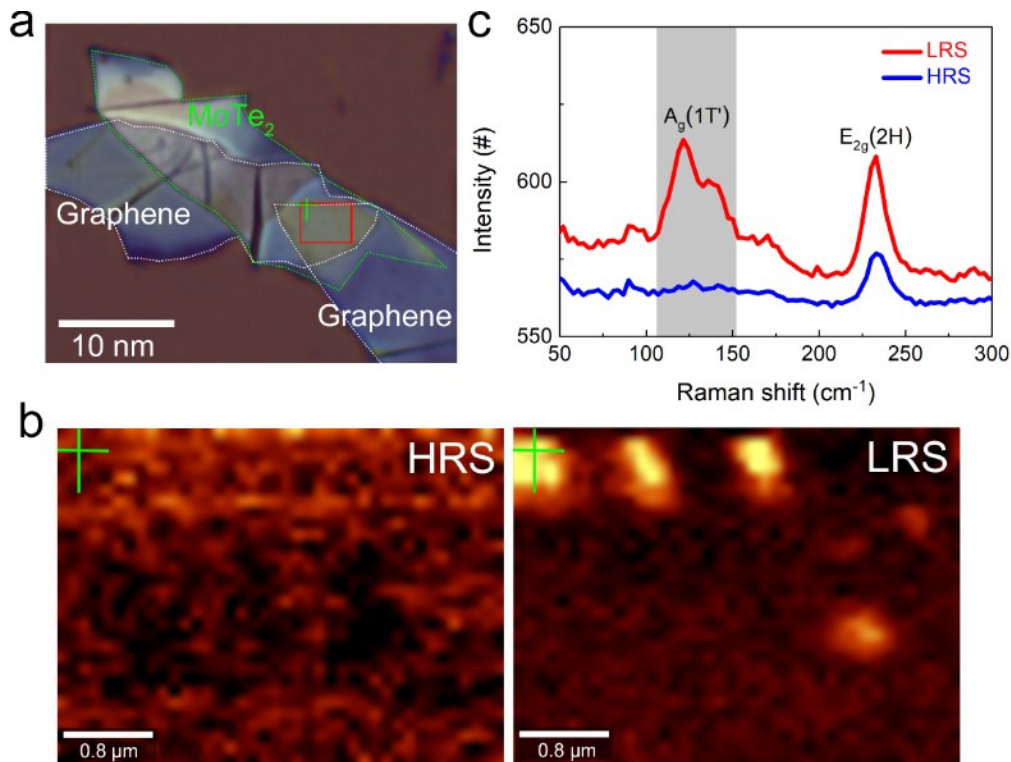


**Fig. S10 In-situ Raman analysis of another sample.** (a) The optical image of the graphene/MoTe<sub>2</sub>/graphene device. The mapping area is marked with a red rectangle. (b) Two Raman maps correspond to the sum of Raman intensity counts in the range of 100.4-150.1 cm<sup>-1</sup> (indicating 1T' phase) at the LRS and HRS. (c) Raman spectra of the position marked with green cross in (b) at the LRS and HRS.

## 9. Auger measurements

According to previous reports, Te metal shows characteristic peaks at ~120 cm<sup>-1</sup> and ~140 cm<sup>-1</sup>, which has similar peak positions to the A<sub>g</sub> mode of 1T'-MoTe<sub>2</sub>. To rule out the possibility of Te metal generation during the switching process, Raman analysis and Auger measurements were employed, as shown in Fig. S11. Fig. S11a shows the optical image of one graphene/MoTe<sub>2</sub>/graphene device. The device was switched to the LRS after electroforming. Then, the top graphene was removed, as shown in Fig. S11b. The Raman and Auger mapping area is marked with a red rectangle. The Raman map was collected based on the sum of Raman

intensity counts in the range of 111.6-148.1  $\text{cm}^{-1}$ . The Raman peaks in the range of 100.4-150.1  $\text{cm}^{-1}$  including peaks at 124 and 138  $\text{cm}^{-1}$ , correspond to the  $A_g$  mode of 1T'-MoTe<sub>2</sub> or characteristic peaks of Te metal. Thus, the bright region in obtained Raman map might stem from 1T'-MoTe<sub>2</sub> or Te metal. Then, the Auger map that collected based on the Auger intensity in 486 eV (Te metal) were employed to check the existence of Te metal. As shown in the right panel of Fig. S11b, there are no obvious bright regions in the Auger map, indicating that the bright region in Raman map is 1T'-MoTe<sub>2</sub> rather than Te metal.

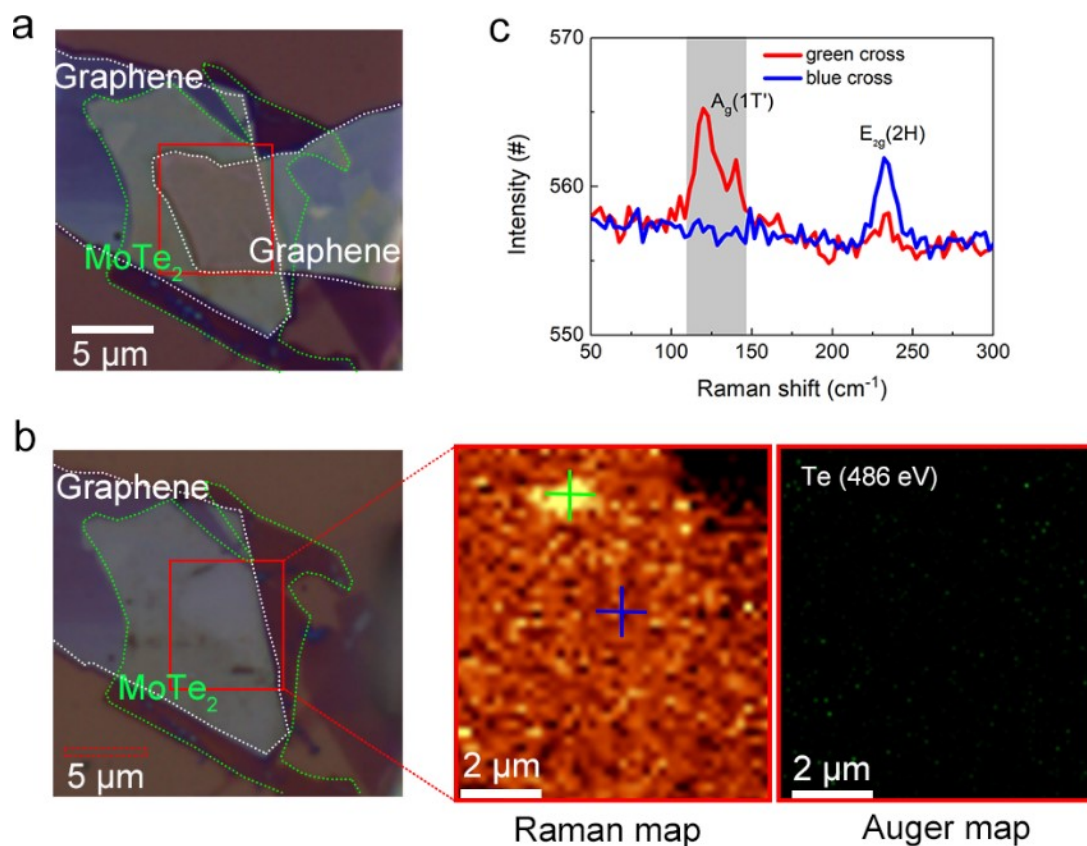


**Fig. S11 Auger measurements.** (a) The optical image of the graphene/MoTe<sub>2</sub>/graphene device.

(b) The optical image of the device without the top graphene. The images on the right are the

Raman map (in the range of 111.6-148.1  $\text{cm}^{-1}$ ) and the Auger map (486 eV). (c) Raman spectra of the positions marked with the green cross and blue cross in the Raman map, respectively.

## 10. In-situ Raman spectra cycles.

In-situ Raman spectra cycles of the phase transition region is employed to verify the reproducibility of the phase transition process. The Raman spectra is collected at the same position in the phase transition region. As shown Fig. Fig. S12, Raman spectra is nearly same in both the HRS and LRS during two  $I$ - $V$  cycles, indicating the relative proportions of 2H and 1T' phases in the phase transition region remain unchanged in both the HRS and LRS.

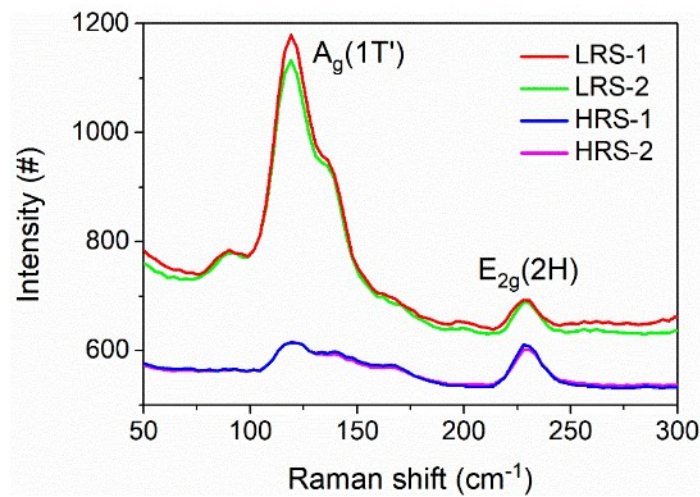


**Fig. S12** Raman spectra of the same position in the phase transition region during two  $I$ - $V$  cycles.

## 11. Temperature-dependent electrical performance

The temperature-dependent electrical performance of the pristine, HRS and LRS states were measured from 80 K to 360 K at a voltage of 0.1 V. These Devices kept their original states during the full temperature range. As shown in Fig. S13, the resistance of the pristine state and HRS states dramatically decrease with the increasing of temperature, indicating a semiconducting behavior. In contrast, the resistance value of LRS states slightly increase, indicating a metallic behavior. These results are consistent with the in-situ Raman measurements and further verify that the switching stems from phase transition between semiconducting 2H phase and metallic 1T' phase.

---

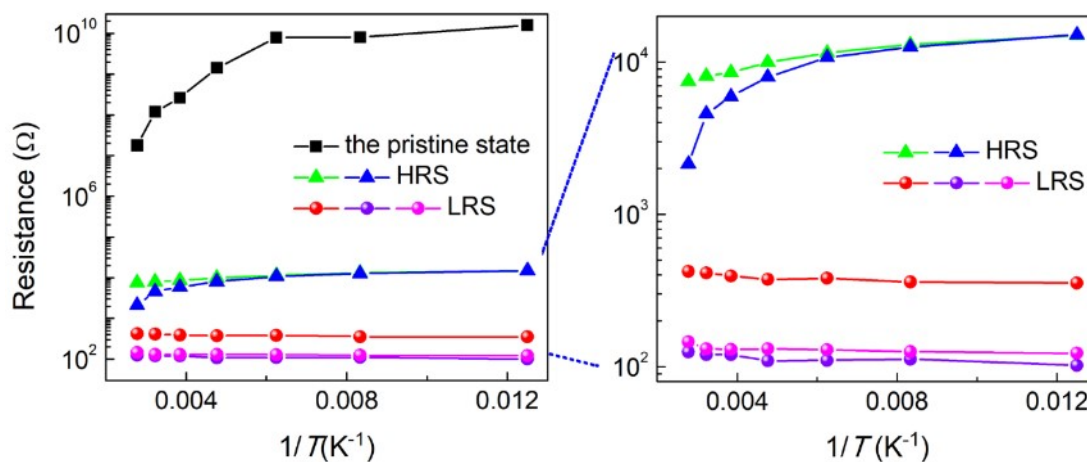


**Fig. S13** Temperature-dependent electrical properties of the intrinsic state (2H phase), the HRS and LRS. The intrinsic state and the HRS states exhibit a semiconducting behavior while the LRS states show a metallic behavior.

## 12. The effect of Ar plasma treatment on the MoTe<sub>2</sub> flake

In addition to Te vacancies shown in Fig. 5E in the maintext, Te vacancies were also observed in other places in the MoTe<sub>2</sub> flake with plasma treatment (Fig. S14).

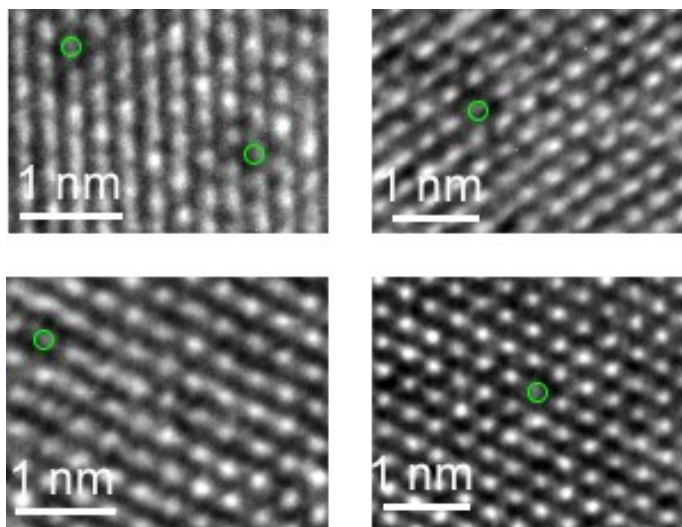


**Fig. S14** Te vacancies in other places in the MoTe<sub>2</sub> flake with Ar plasma treatment. Te vacancies are indicated by green hollow circles.

### 13. The 2H-to-1T' phase transition achieved through collective transversal sliding

The 2H-to-1T' phase transition is achieved through collective transversal sliding of a whole Te atomic layer to the hollow sites (Fig. S15).

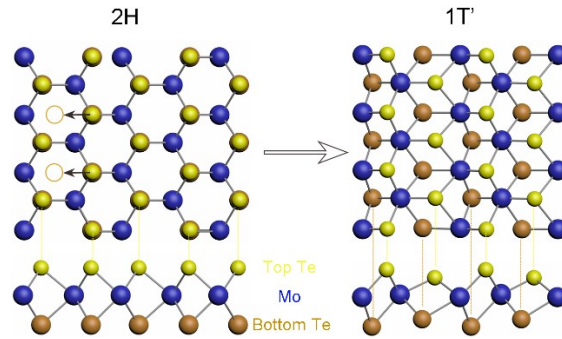


**Fig. S15** The 2H-to-1T' phase transition achieved through collective transversal sliding.

### 14. The effect of plasma treatment parameter on the structure of MoTe<sub>2</sub> and the resistive switching behaviors

When the treatment power increased to 80 W, the structure of the MoTe<sub>2</sub> flake was destroyed (Fig. S16). Thus, high treatment power should be avoided during the device fabrication.

The plasma treatment time greatly affects the concentration of Te vacancies, that is, the longer the treatment time, the more Te vacancies generated. Fig. S17 reports electrical performance of the MoTe<sub>2</sub> devices with treatment time of 80, 150 and 300 s, and the treatment power is fixed at 20 W. As shown in Fig. S17a and Fig. S17b, the forming voltage and the SET voltage reduced when the treatment time increased since much more Te vacancies formed. For devices with treatment time of 80 and 150 s, their switching behaviors are similar, including forming voltage, SET voltage and ON/OFF ratio. However, the switching behavior is unstable when the treatment time is 80 s, as shown in Fig. S18a. This is because the concentration of Te

---

vacancies is not enough to significantly reduce the switching energy between 2H and 1T' phases. In contrast, the device with treatment time of 300 s performs relatively small ON/OFF ratio, and is easily stuck in the LRS after several cycles (see Fig. S18b). The reason is that too much Te vacancies generate, leading to easily stuck in 1T' phase. Thus, the optimal plasma treatment condition is 20 W/150 s.

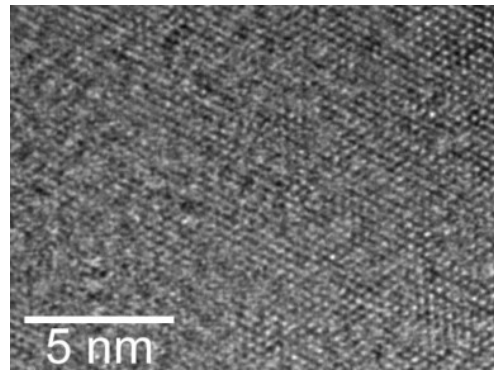


**Fig. S16** HRTEM image of the MoTe<sub>2</sub> flake with the treatment power of 80 W.

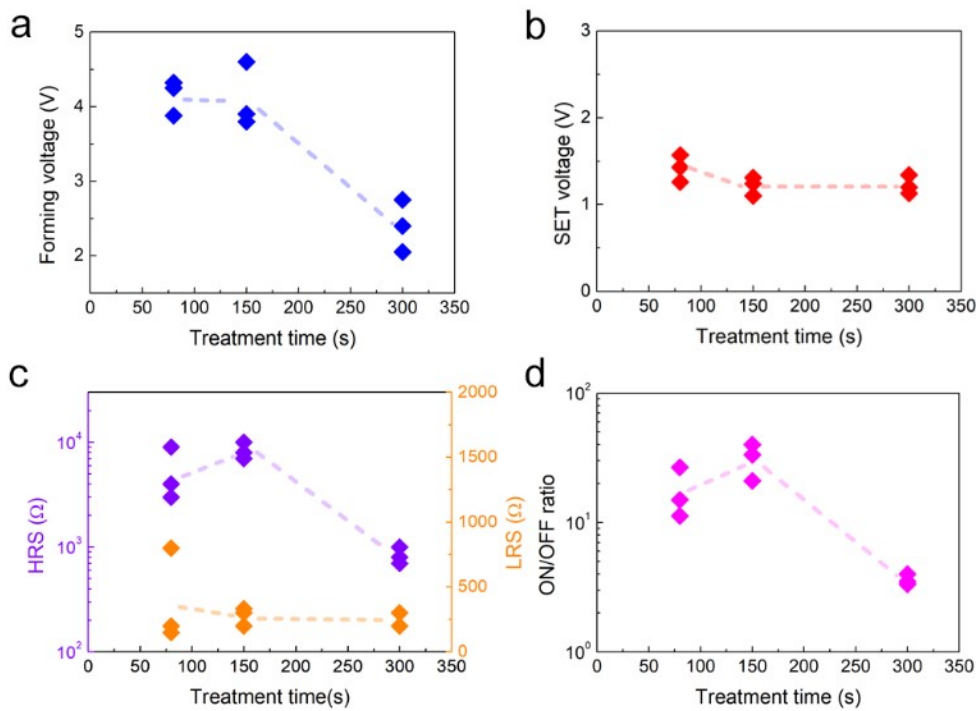


**Fig. S17** The electrical performance of the MoTe<sub>2</sub> devices with different treatment times, including forming voltage (a), SET voltage (b), HRS and LRS (c) and ON/OFF ratio (d). The treatment power is fixed at 20 W.

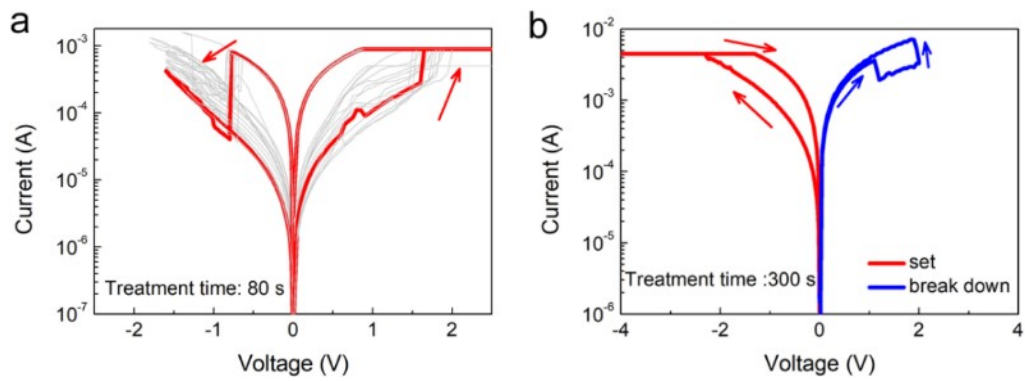


**Fig. S18** Switching behaviors of the MoTe<sub>2</sub> devices with treatment time of 80 s (a) and 300 s (b).

Table S1 summarizes electrical performance of the devices with different treatment times.

**Table**

**Table S1. Electrical performance of the MoTe<sub>2</sub> devices with different treatment times.**

Treatment time (s)	80 s	150 s	300 s
Forming voltage (V)	4-5 V	4-5 V	2-3 V
SET voltage (V)	1-2 V	1-2 V	1-2 V
HRS/LRS ( $\Omega$ )	$10^4/10^2$	$10^4/10^2$	500/200
ON/OFF ratio	>10	>10	2-3
RS performance	Not stable	stable	Easily break down